IEEE Access
Multidisciplinary ⋮ Rapid Review ⋮ Open Access Journal

Received 8 March 2023, accepted 3 April 2023, date of publication 6 April 2023, date of current version 17 April 2023.

Digital Object Identifier 10.1109/ACCESS.2023.3265326

APPLIED RESEARCH

Modeling and Detection of Dynamic Position Sensor Offset Error in PMSM Drives

SANDUN S. KURUPPU[1], (Senior Member, IEEE), SUNIL G. ABEYRATNE[2], (Senior Member, IEEE), AND SANDUN HETTIARACHCHI[2]

[1]Department of Electrical and Computer Engineering, Western Michigan University, Kalamazoo, MI 49008, USA
[2]Department of Electrical and Electronics Engineering, University of Peradeniya, Peradeniya 20400, Sri Lanka

Corresponding author: Sandun S. Kuruppu (sandun.kuruppu@wmich.edu)

This work was supported in part by the Ruth and Ted Braun Fellowship at Saginaw Valley State University.

ABSTRACT Rotor position information obtained through a position sensor is crucial for proper field-oriented control (FOC) of permanent magnet synchronous machine-based high dynamic energy conversion applications. In applications such as transportation and industrial, PMSM energy conversion systems are subjected to harsh environmental conditions such as vibration, shock, and thermal shock causing mechanical interfaces holding position sensors to fail, introducing errors to the position measurement. A dynamic position sensor offset error (DPSOE), being such a failure mode has the potential to degrade system torque output or more adversely, reverse machine torque output that may cause catastrophic outcomes. This paper evaluates different DPSOE scenarios, presents an approach to model the failure mode for analysis and proposes two novel, and robust DPSOE detection methods for PMSM drive systems. The proposed detection methods are analytically proven and supported by simulation and experimental results under multiple operating conditions proving robustness.

INDEX TERMS Permanent magnet synchronous motors, position measurement, fault detection, machine vector control, brushless machines.

I. INTRODUCTION

Electromechanical energy conversion now and again has proven to be superior in numerous aspects when compared with conventional non-electromechanical energy conversion systems such as hydraulic systems and internal combustion engines. Improved efficiency, higher torque/power density, reduced maintenance requirements, and ease of interfacing with software-based controls are some of the key factors contributing to electrification of actuation systems across a broad set of applications. More recently, the aviation industry has shown a strong interest in electrification considering the extravagant benefits [1], [2], [3].

Energy efficiency being a key metric across numerous industries (transportation, industrial, and residential), permanent magnet synchronous machines (PMSMs), surpass other machine types in terms of efficiency. Other factors such as compact design, ease of optimal torque generation through field orientation, ease of thermal management, and reliability have led to PMSMs being the preferred electromechanical energy conversion device, despite the cost associated with permanent magnets. Growing sectors such as autonomous driving, powertrain electrification, and aviation electrification are leaning towards PMSM-based energy conversion attributed to their superior performance compared to other electric machines [4], [5].

In applications, PMSMs are used as torque controllers, speed controllers, or position controllers. Despite the final control variable, a PMSM requires rotor position information for proper field-oriented control (FOC), and this is achieved either with a position sensor, or with an algorithm that estimates rotor position (i.e., sensorless position sensing). Though a sensor-based PMSM FOC control strategy is costly, it is far superior to sensorless control strategies for applications involving high load/torque dynamics [6], [7], [8].

The associate editor coordinating the review of this manuscript and approving it for publication was Shaopeng Wu.

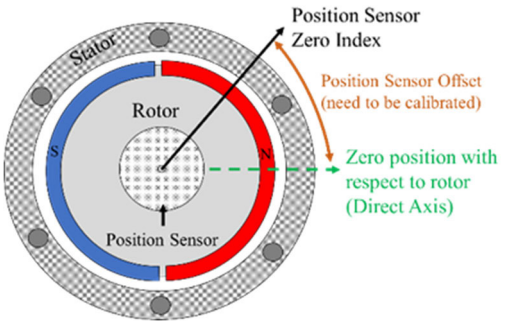

FIGURE 1. Position sensor offset error from a motor cross-section.

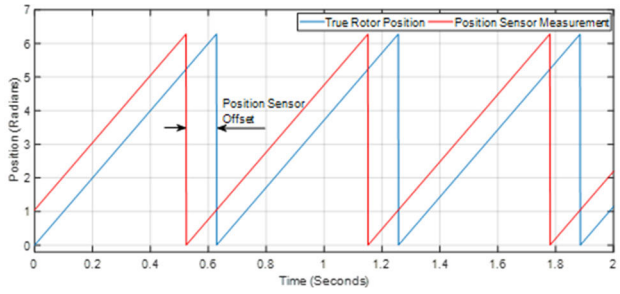

FIGURE 2. Position sensor offset error based on sensor measurement.

Rotor position sensing in PMSMs is commonly achieved through optical encoders, resolvers, or linear hall sensors. Despite the type of sensor technology, some form of mechanical interfacing between the sensor and the motor is required. Each sensor includes a rotor-mounted element and a stator-mounted element. The relative motion between these two elements is used to determine the rotor position with respect to the stator. Once assembled onto the motor, these sensors require two sets of calibrations [9], [10], [11], [12]. Of them, the first is the position sensor offset calibration or the back emf offset calibration that allows the proper alignment between position sensor zero and rotor zero position as shown in figures 1 and 2 below.

Since the position sensors are mechanically mounted on the stator and rotor of a machine, these mechanical assemblies have the potential to fail due to aging, rapid acceleration/deceleration, manufacturing defects, thermal cycling, thermal shock, and/or vibration. The dynamic position sensor offset error (DPSOE) fault, presented in this paper is the failure of the mechanical interface holding the sensor, introducing a time varying position sensor offset that is unpredictable.

The effect of such failure poses harmful system response such as stall conditions, torque reversal, or reduced torque output [13]. The effect of inaccurate position sensor offset calibration from a static offset point of view has been discussed in detail in [13]. However, a mechanical failure in a rotating system is dynamic in nature and not only a Static PSOE (SPSOE). Despite position sensors being a crucial element in the reliable operation of a PMSM system, position sensor failure modes are often overlooked [14]. Existing literature that may relate to position sensor faults is discussed herewith illustrating DPSOE is not addressed in the existing literature. Resolver single-phase fault-tolerant approach is proposed in [15], where the faulted signal is reconstructed based on healthy signals. Authors of [16] propose a position and speed estimation approach that combines high-frequency injection with discrete hall sensor inputs. However, this approach is not appropriate for torque control applications due to the inaccuracy of position signal information at stall conditions nor addresses DPSOE. A DC bus current sensor-based position sensor fault detection is presented in [17]. The proposed approach computes three-phase currents based on DC bus current measurements and voltage vector applied. However, a DPSOE will adversely influence the current estimation strategy as the currents are referred to from an incorrect frame of reference, making the proposed approach impractical for DPSOE fault. A multi-fault diagnosis is proposed in [18] where IGBT, current sensor, and speed sensor fault diagnosis is performed. However, this approach also assumes that accurate rotor position information is available for fault diagnosis. The hall effect sensor fault detection proposed in [19] is only applicable to discrete hall sensors in trapezoidal controlled drives. Therefore, the approach is not practical for linear position sensors used in FOC drives.

Noting the gap in the literature on DPSOE fault detection, this paper presents the following.

1). How a DPSOE may behave in an FOC system
2). An approach to model failure mode characteristics
3). Robust DPSOE detection strategies

The organization of the rest of the paper is as follows. Section II outlines the challenges associate with DPSOE. Variations of DPSOE fault are discussed in section III, followed by a model to replicate these different variations in simulation. Section IV proposes a detection strategy to detect a DPSOE condition followed by simulation and experimental results in section V. Section VI outlines an alternate method with reduced computations for DPSOE detection followed by the conclusion of the paper.

The main contributions of this paper include the presentation of DPSOE fault model and two fault diagnosis methods. The first method proposed in section IV allows for an accurate quantification method which requires more computational power. The alternate method discussed in section IV is a simpler method that only allows fault detection without the ability to quantify the fault severity. As discussed in the literature review, modeling, detection nor severity assessment of DPSOE fault diagnosis is not available in present body of knowledge and this paper makes a significant contribution.

II. PROBLEM STATEMENT AND KEY CHALLENGES

The primary difference that makes DPOSE a challenging problem is that during a DPSOE fault, the motor speed and position signals measured by the actuator experiencing the fault are sporadic and unpredictable. In contrast, the speed measured during an SPSOE fault is accurate, attributing to the constant offset in the rotor positions measurement. The measured rotor position $\theta_m(t)$, true rotor position $\theta_r(t)$, and PSOE $\Delta\theta(t)$ are related as shown in (1). Since the speed

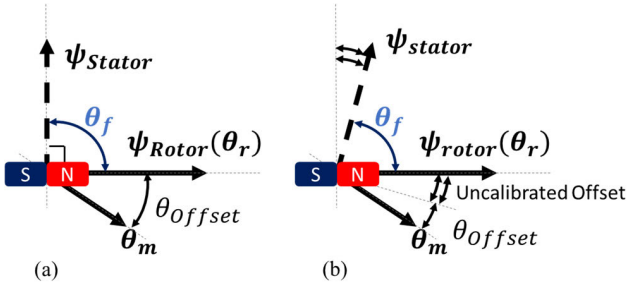

FIGURE 3. PMSM FOC flux vector placement under non-faulty and faulty position sensor offset.

is obtained by differentiating position, the measured speed $\omega_m(t)$, actual rotor speed $\omega_r(t)$, and the influence of PSOE on speed measurement may be derived as (2). In SPSOE $\Delta\theta\ (t)$ is constant and $\dot{\Delta\theta}\ (t) = 0$, while during DPSOE $\Delta\theta\ (t)$ is time- varying and $\dot{\Delta\theta}\ (t)$ is non-zero.

$$\theta_m(t) = \theta_r(t) + \Delta\theta(t) \tag{1}$$

$$\omega_m(t) = \omega_r(t) + \dot{\Delta\theta}(t) \tag{2}$$

A DPSOE fault poses a severe risk to users, property, and the system itself due to the unintended and unpredictable nature of the torque response. The following discussion emphasizes the criticality of DPSOE fault from an FOC PMSM system utilized in torque control applications to explain to the reader the need for fault detection. In field-oriented control of PMSMs, the rotor flux vector alignment/position is measured or estimated to optimally place the stator flux vector. The stator flux vectors rotate at a speed different to that of the rotor flux vector speed when DPSOE is present.

In figure 3.a, a non-faulty position sensor offset is shown where the relative angular alignment between the rotor flux vector and the stator flux vector is known and constant. Therefore, enables the optimal placement of the stator flux vector with respect to the rotor flux vector. Figure 3.b is a faulty sensor where there is an uncalibrated offset error which is varying under rotor movement due to a loosened position sensor. These fluctuations in the position offset cause the rotor flux vector to be placed mostly non-optimally resulting in reduced torque, zero torque, or torque reversal. Simulation, and experimental results presented earlier corroborate this conclusion. Apart from the loss of torque and torque reversal, the masking of the fault by the closed-loop control system makes this fault one of the more severe faults in PMSM FOC drives that require attention. In current regulated PMSM FOC drives, the current regulation continues to regulate the current in the incorrect frame of reference during PSOE as the current references are unable to distinguish between a correct and an incorrect position signal [13]. As demonstrated with experimental results, FOC controlled PMSM continues to operate with DPSOE without drive overcurrent fault or any other hardware faults. Hence rapid detection of this fault is of utmost importance.

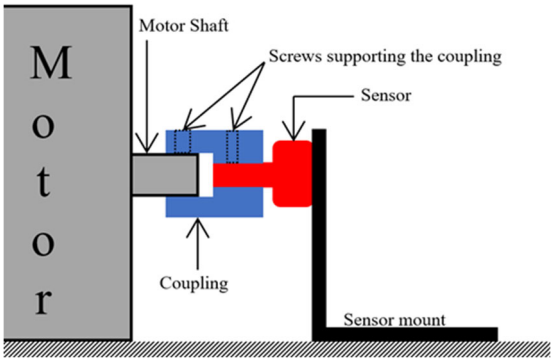

FIGURE 4. DPSOE behavior test platform diagram.

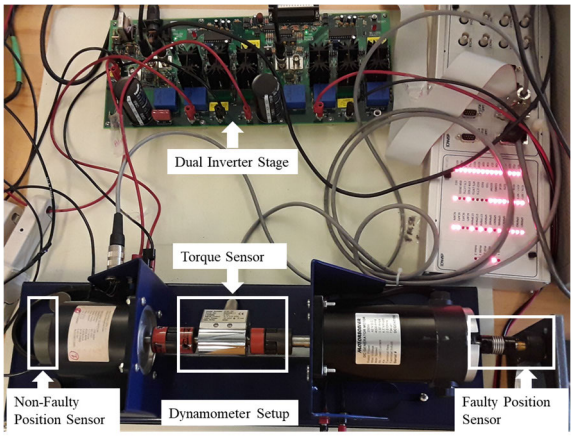

FIGURE 5. Experimental test platform for DPSOE behavior study.

III. BEHAVIOUR AND MODEL OF DYNAMIC POSITION SENSOR OFFSET ERROR

A. OBSERVING THE BEHAVIOUR OF DPSOE

The experimental DPSOE fault injection setup depicted in figure 4 was developed and added to the dynamometer setup shown in figure 5 to study system behavior during DPSOE and to facilitate accurate model development. The dynamometer setup consists of a PMSM, and DC motor. The DC motor consists of a position sensor and with the ability to be driven under various modes (torque control, speed control and position control) and under various profiles of operation. The position sensor mounted on the DC motor is utilized as the faulty sensor facilitating the study of DPSOE behavior under various operation modes.

DPSOE is introduced by loosening the screws holding the coupling that couples the sensor to the motor shaft. The experimental evaluation demonstrated three primary fault modes of DPSOE.

- Stick-slip behavior (Figure 6)
- Completely stuck behavior (Figure 6)
- Continuous slip behavior (Figure 7)

The three primary behaviors of DPSOE stem from the level of coupling between the motor rotor/shaft, and the rotating portion of the position sensor. When the position sensor is rigidly coupled to the motor rotor, the speed of the motor rotor (ω_r) is equal to the speed of the sensor (ω_m), while maintaining the difference between the absolute position zero

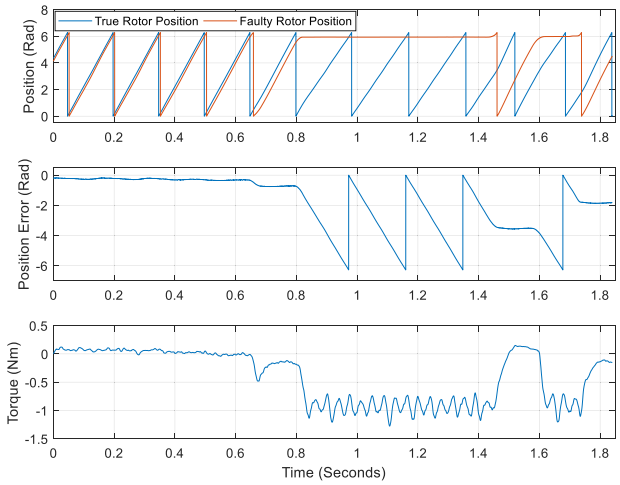

FIGURE 6. Experimental results on stick-slip and stuck behavior.

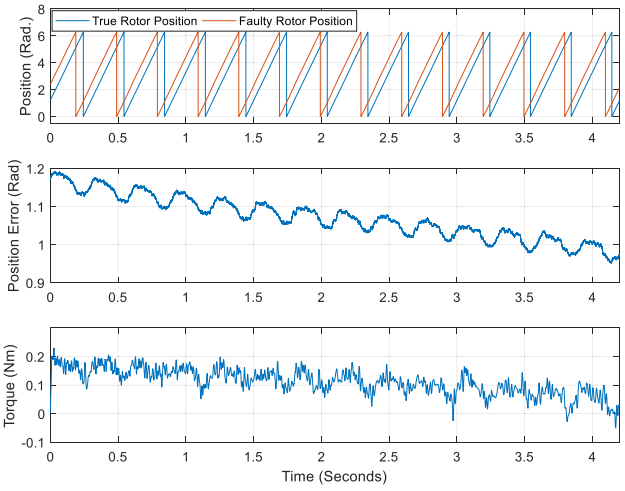

FIGURE 7. Experimental results on continuous slip behavior.

locations of the sensor and the rotor constant. In other words, the position sensor is following the motor rotor at a known, constant/static PSOE. A continuous slip behavior is when ω_r is not equal to ω_m and ω_m is non-zero. The stick-slip behavior is when ω_m is equal to ω_r, for some period and the speeds are not equal at other times. The completely stuck sensor behavior is when ω_m is zero where as ω_r is non-zero. Experimental results for each of these three fault scenarios are depicted in figures 6 and 7. Each figure illustrates the behavior of rotor position (θ_r), measured position with the faulty/loosened sensor (θ_m), the difference between the two position signals (DPSOE) and FOC PMSM torque output. The sporadic nature of the torque output of the PMSM under DPSOE is apparent demonstrating the severity of the fault. Considering experimental results, the following relationship may be obtained for DPSOE.

$$\theta_r(t) = \int \omega_r(t)\,dt + \theta_{r0} \tag{3}$$

$$\theta_m(t) = \int \omega_m(t)\,dt + \theta_{m0} \tag{4}$$

$$\theta_r(t) - \theta_m(t) = \int [\omega_r(t) - \omega_m(t)]\,dt + \theta_{r0} - \theta_{m0} \tag{5}$$

The reasoning for the DPSOE model approach is presented in the following discussion. As discussed earlier, any type of position sensor consists of a rotor-mounted element and a stator-mounted element. The relative motion between the two elements enables rotor position measurement. For example, in a hall effect sensor, the magnet is mounted on the rotor and the sensor is mounted on the stator, or in an optical encoder, the disk is mounted on the rotor whereas the light source and the sensor are mounted on the stator. The rotor-mounted element is held mechanically through friction. A failure in the mechanical interface may result in a permanent shift in the mounting location, intermittent shift in the mounting location, partial breakage, or complete breakage, leading to the following scenarios. A permanent shift in the mounting location is a static PSOE, which has been discussed in previous literature. An intermittent shift (also known as stick-slip behavior) in the mounting location is caused by a lack of 'sensor holding friction torque' (T_{SHFT}) under rapid accelerations and decelerations to hold the sensor in place (figure 6). However, in this scenario the T_{SHFT} is sufficient to hold the sensor in place under low acceleration/deceleration movements. The second intermittent shift scenario for the sensor mount location is caused by the T_{SHFT} being significantly low causing slow rates of acceleration to introduce motion to the rotor- mounted element (figure 7). A complete breakage causes the T_{SHFT} to be zero allowing the sensor to move sporadically based on the 'jerk' transferred from the motor rotor (figure 6). The temperature of the overall system, and the sensor module elements may also influence T_{SHFT}, (level of material expansion resulting in a loosened sensor), but not discussed in this paper.

B. MODELING OF DPSOE BEHAVIOR

In summary, the sensor element on the rotor requires sufficient holding torque from the mounting interface. Due to various degrees of mechanical failure, at times the sensor is completely coupled to the motor rotor, and there may be occasions where the coupling is partially, or fully decoupled.

Depending on the level of coupling, the amount of torque transferred (full, partial, or no torque transferred) from the motor shaft to the sensor element on the rotor vary. Further, depending on the level of coupling of the sensor element to the motor shaft, the inertia influencing the motion of the loosened sensor also varies. In summary, the dynamics of the sensor are governed by the combined inertia of the motor rotor and the sensor inertia or solely by the inertia of the sensor element only. The collective effect of the amount of torque transferred and the effective inertia, influence the DPSOE behavior. Considering these factors, the DPSOE model shown in figure 8 was developed.

FOC-based torque controlled PMSM and drive system in a speed-regulated dynamometer (DC machine) is depicted in figure 8 above, elaborating sensor coupling failure. The coupling between the PMSM and the DC machine is assumed to be rigid. The model for mechanical dynamics with and without DPSOE is shown in the dashed box within figure 8.a.

This model allows the evaluation of true rotor position along with measured position from the faulty sensor. Equation (6) holds under a no-fault scenario and once the sensor if properly offset calibrated, $\theta_r(s) = \theta_m(s)$. J_{mech}, J_{snsr} are mechanical system inertia excluding the sensor inertia and sensor inertia (inertia of the sensor element on the rotor), respectively. B_{mech}, B_{snsr} are viscous friction/damping coefficients of the mechanical system, excluding the sensor and sensor itself. T_{em}, T_L are electromagnetic torque from the PMSM and dynamometer load respectively, assuming friction torque is negligible.

$$\theta_r(s) = \frac{1}{s}\left[\frac{T_{em} - T_L}{(J_{mech} + J_{snsr})\,s + (B_{mech} + B_{snsr})} + \omega_{r0}\right] + \theta_{r0} \tag{6}$$

The measured and true rotor position under DPSOE is shown below in equations 7 and 8.

$$\theta_r(s) = \frac{1}{s}\left[\frac{(T_{em} - T_L)\,(1 - T\_fractional)}{(J_{mech})\,s + (B_{mech})} + \omega_{r0}\right] + \theta_{r0} \tag{7}$$

$$\theta_m(s) = \frac{1}{s}\left[\frac{(T_{em} - T_L)\,T\_fractional}{(J_{snsr})\,s + (B_{snsr})} + \omega_{m0}\right] + \theta_{m0} \tag{8}$$

$'T\_fractional'$ represents the fraction associated with scaling the amount of torque transferred from the motor rotor to the loosened sensor module based on the T_{SHFT}. The behavior of this time-varying torque depends on the degree of motor rotor surface contact made during the respective DPSOE fault mode (i.e., continuous slip, stick-slip, or completely stuck). The '*Intermittent Fault*' signal (shown in red in the model implementation) in the model allows emulation of the intermittent behavior of DPSOE. Subfigures (b) and (c) of figure 8 illustrate the attached and detached modes of the position sensor from the motor rotor.

C. MODEL VALIDATION THROUGH SIMULATION RESULTS

The DPSOE model proposed earlier is validated through simulation results to compare with the experimental results shown earlier. Stick-slip behavior, completely stuck, and continuous slip behavior in simulation are presented in figures 9 and 10. The modeled faulty sensor behavior and the motor control system with the faulty sensor closely follow the results obtained experimentally.

IV. DERIVATION OF DPSOE DETECTION AND QUANTIFICATION IN PMSM FOC DRIVES

In order to devise a DPSOE detection strategy, the current regulation-based field-oriented controlled PMSM shown in figure 8 is represented in a block diagram form as a multi-input multi-output system in figure 11.

Here, $I^r_{qs\_ref}$ and $I^r_{ds\_ref}$ are current commands applied to the closed loop system. C(s) is the matrix containing proportional and integral regulators (PI regulators) for quadrature and direct axis as shown in (9). K_P and K_I are proportional and integral gains of the controller. 's' represents the Laplace variable. θ_r is the true motor rotor position while θ_m is the rotor position measured by the erroneous sensor under DPSOE fault. $K_s(\theta)$ and $K'_s(\theta)$ are forward and inverse rotor reference frame transformations respectively. P(s) is the inverse motor model where, L_q, and L_d, are inductances along each axis while r_s and ω_r represent resistance and rotor speed, respectively. V^r_{qs} and V^r_{ds} are rotor reference frame voltages applied by the FOC controller but observed from the motor reference frame. $L_q \approx L_d$ is appropriate as a non-salient machine is considered.

$$C(s) = \begin{bmatrix} (K_P s + K_I)/s & 0 \\ 0 & (K_P s + K_I)/s \end{bmatrix} \tag{9}$$

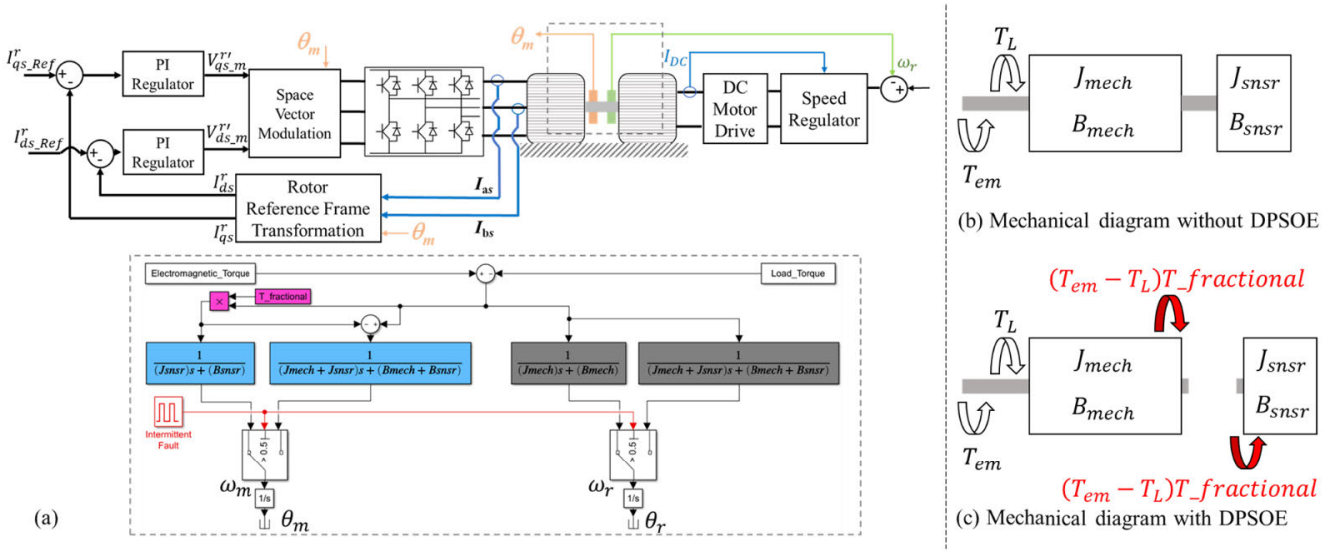

FIGURE 8. Modeling the DPSOE behavior with PMSM torque actuator and speed regulator dynamometer.

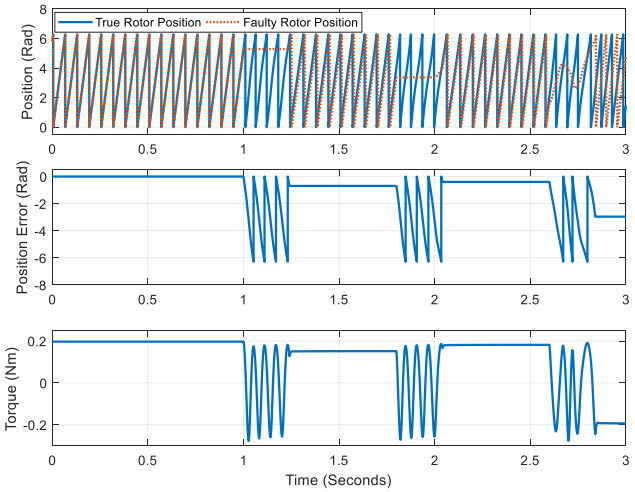

FIGURE 9. Simulation of stick-slip and stuck behavior of position sensor.

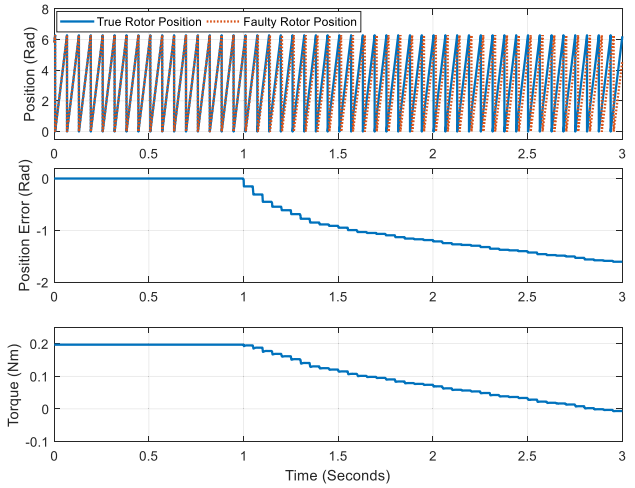

FIGURE 10. Simulation of continuous slip behavior of position sensor.

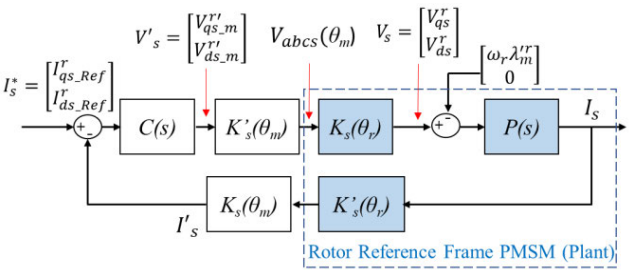

FIGURE 11. Block diagram of field-oriented controlled PMSM.

$$K_s(\theta) = \frac{2}{3}\begin{bmatrix} \cos(\theta) & \cos\left(\theta - {}^{2\pi}/_{3}\right) & \cos\left(\theta + {}^{2\pi}/_{3}\right) \\ \sin(\theta) & \sin\left(\theta - {}^{2\pi}/_{3}\right) & \sin\left(\theta + {}^{2\pi}/_{3}\right) \end{bmatrix} \tag{10}$$

$$K_s'(\theta) = \begin{bmatrix} \cos(\theta) & \sin(\theta) \\ \cos\left(\theta - {}^{2\pi}/_{3}\right) & \sin\left(\theta - {}^{2\pi}/_{3}\right) \\ \cos\left(\theta + {}^{2\pi}/_{3}\right) & \sin\left(\theta + {}^{2\pi}/_{3}\right) \end{bmatrix} \tag{11}$$

$$P(s) = \begin{bmatrix} r_s + sL_q & \omega_r L_d \\ -\omega_r L_q & r_s + sL_d \end{bmatrix}^{-1} \tag{12}$$

By applying superposition theorem to the above closed loop system, the following result is obtained for the voltages applied by the controller under dynamic state.

$$V'_s = \frac{C(s)}{\left[I + C(s)T^{-1}P(s)\,T\right]} I_s^* + \frac{C(s)T^{-1}P(s)}{\left[I + C(s)T^{-1}P(s)\,T\right]} \times \begin{bmatrix} \omega_r \lambda'^r_m \\ 0 \end{bmatrix} \tag{13}$$

where,

$$T = K_s(\theta_r)\,K_s'(\theta_m) \tag{14}$$

The following result is obtained by simplifying the results in (13) under steady state conditions where,

$$\begin{bmatrix} V'^r_{qs\_m} \\ V'^r_{ds\_m} \end{bmatrix} = \begin{bmatrix} r_s & \omega_r L_d \\ -\omega_r L_q & r_s \end{bmatrix} \begin{bmatrix} I^r_{qs\_Ref} \\ I^r_{ds\_Ref} \end{bmatrix} + \begin{bmatrix} \cos(\Delta\theta) \\ -\sin(\Delta\theta) \end{bmatrix} \omega_r \lambda'^r_m \tag{15}$$

Existing literature utilizes the above result along with a motor model to extract the induced emf contributions along quadrature and direct axis under a static PSOE (SPSOE) [13]. However, the approach used for SPSOE diagnosis is not applicable under a DPSOE as the motor speed calculated based on the faulty position sensor is inaccurate. Hence the following approach is proposed. The result in (15) is rewritten as (16) and (17).

$$V'^r_{qs\_m} - r_s I^r_{qs_{Ref}} = \omega_r L_d I^r_{ds_{Ref}} + \cos(\Delta\theta)\,\omega_r \lambda'^r_m \tag{16}$$

$$V'^r_{ds\_m} - r_s I^r_{ds_{Ref}} = -\omega_r L_q I^r_{qs_{Ref}} - \sin(\Delta\theta)\,\omega_r \lambda'^r_m \tag{17}$$

PMSMs where $\lambda'^r_m / L_q \gg \sqrt{\left(I^r_{qs_{Ref}}\right)^2 + \left(I^r_{ds_{Ref}}\right)^2}$, allows for the inductive voltage drop to be assumed negligible. In non-salient PMSMs, the reader may use the larger of the two inductance values, L_q and L_d. Hence, (16) and (17) maybe re-written as (18) and (19).

$$V'^r_{qs\_m} - r_s I^r_{qs_{Ref}} = \omega_r L_d \left(I^r_{ds_{Ref}} + \cos(\Delta\theta)\,\lambda'^r_m / L_d\right) \tag{18}$$

$$V'^r_{ds\_m} - r_s I^r_{ds_{Ref}} = -\omega_r L_q \left(I^r_{qs_{Ref}} + \sin(\Delta\theta)\,\lambda'^r_m / L_q\right) \tag{19}$$

Considering the inequality discussed previously, (18) and (19) is reduced to (20) and (21), respectively. The approximation results in a speed-independent DPSOE diagnosis strategy and the authors will show that the approximation has minimal impact on detecting a DPSOE, in the following sections. $V^r_{qs\_error}$ and $V^r_{ds\_error}$ are quantities computer within a microprocessor to assist in the calculation of $\Delta\theta\,(t)$, as shown in (22).

$$V^r_{qs\_error} = V'^r_{qs\_m} - r_s I^r_{qs_{Ref}} \approx \cos(\Delta\theta)\,\omega_r \lambda'^r_m \tag{20}$$

$$V^r_{ds\_error} = V'^r_{ds\_m} - r_s I^r_{ds_{Ref}} \approx -\sin(\Delta\theta)\,\omega_r \lambda'^r_m \tag{21}$$

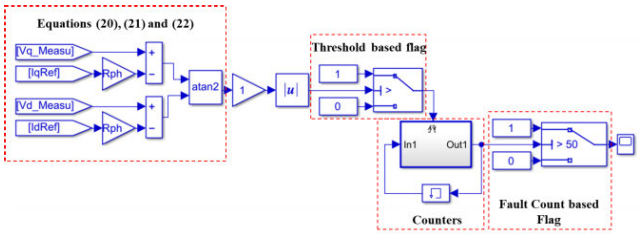

FIGURE 12. Block diagram of the DPSOE detection with inverse tangent calculation.

The above result now can be used for the approximate quantification of DPSOE without the need for accurate motor rotor speed as shown in (22), followed by the detection strategy.

$$\Delta\theta\,(t) = \tan^{-1}\left(-V^{r}_{ds\_error} \Big/ V^{r}_{qs\_error}\right) \tag{22}$$

The following method is proposed for the detection of a DPSOE fault, considering (20), (21), and (22). The approach relies on an inverse tangent calculation to closely approximate the amount of position sensor offset under a DPSOE fault.

A Simulink-based implementation of the proposed method is shown in figure 12. The quantified DPSOE is observed at the output obtained by implementing (22). This value under healthy operation is zero at steady-state. As the sensor moves (i.e., DPSOE fault), the quantified DPSOE oscillates between zero and 2π (or $-\pi$ to π) as shown in figures 9 and 10. The first threshold-based counter compares the absolute value of the quantified DPSOE signal against a preset threshold to evaluate if a DPSOE is present. The same counter converts the quantified DPSOE to a digital signal indicating if a fault is detected or not. The discretization allows the evaluation of how long the fault persists avoiding false positives under transient states (during no fault or healthy state). The second counter assists in tracking the faulty position sensor oscillation cycles about the rotor and compares them with a set count value to indicate a DPSOE fault. Details associated with threshold selection and counter-level selection is discussed below.

The selection of fault detection threshold and counter value are important to allow for proper detection of DPSOE and to avoid false positives under transient conditions. First, the threshold selection for the '*Threshold based flag*' block from figure 12 is discussed. During healthy operation, $\Delta\theta = 0$. Therefore, equations (16) and (17) become, (23) and (24).

$$V^{r'}_{qs\_m} = r_s I^{r}_{qs_{Ref}} + \omega_r L_d I^{r}_{ds_{Ref}} + \omega_r \lambda^{'r}_{m} \tag{23}$$

$$V^{r'}_{ds\_m} = r_s I^{r}_{ds_{Ref}} - \omega_r L_q I^{r}_{qs_{Ref}} \tag{24}$$

Therefore, equation (22) becomes (25).

$$\Delta\theta\,(t) = \tan^{-1}\left(\omega_r L_q I^{r}_{qs_{Ref}} \Big/ \omega_r L_d I^{r}_{ds_{Ref}} + \omega_r \lambda^{'r}_{m}\right) \tag{25}$$

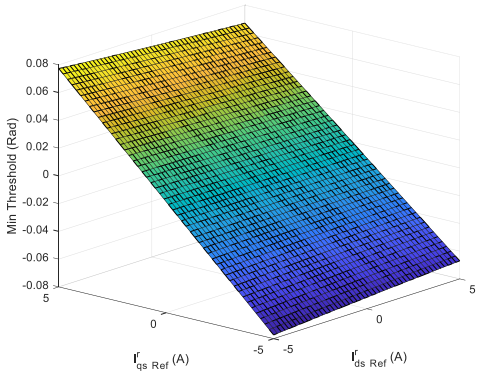

FIGURE 13. Minimum threshold required at current reference under healthy operation to avoid false positives.

The above relationship further reduces to (26).

$$\Delta\theta\,(t) = \tan^{-1}\left(L_q I^{r}_{qs_{Ref}} \Big/ L_d I^{r}_{ds_{Ref}} + \lambda^{'r}_{m}\right) \tag{26}$$

A surface plot is generated considering the range of current references and machine parameters to visualize the detection signal variation range for the chosen experimental setup (figure 13). The figure shows that under healthy conditions, and steady-state, the quantified DPSOE will not exceed ± 0.08 Radians. Therefore, the designer may choose the threshold to be larger than 0.08 in this application/system.

The second component in the algorithm is the counter value to avoid fault positives during transient conditions. The factors considered for transient bypass are closed-loop system bandwidth ($\boldsymbol{\omega_{BW}}$) and the closed-loop system time constant ($\boldsymbol{\tau}$) and the closed-loop system time constant $\boldsymbol{T_s}$ is the sampling rate of the system and the FOC algorithm is expected to execute at every sampling instance. Based on (26), the threshold derived for experimental validation was 100 counts and the selection has proven to be practical.

$$Fault\ Count = {}^{\omega_{BW}}\Big/_{T_s} \tag{27}$$

The reader should note that the proposed approach is for a dynamically varying PSOE rather than a stuck sensor with an incorrect PSOE (i.e., SPSOE). The detection of a static PSOE (SPSOE) is discussed in [13]. Simulation and experimental results pertaining to the proposed DPSOE detection strategy is presented next.

V. SIMULATION AND EXPERIMENTAL RESULTS ON DPSOE DETECTION

A. SIMULATION RESULTS ON DPSOE FAULT DIAGNOSIS

This section presents simulation results on how the proposed fault diagnosis signals behave during a DPSOE fault event and the effectiveness of the proposed strategy under various operating conditions. The simulations were conducted with MATLAB Simulink with machine parameters matching that of the experimental setup used.

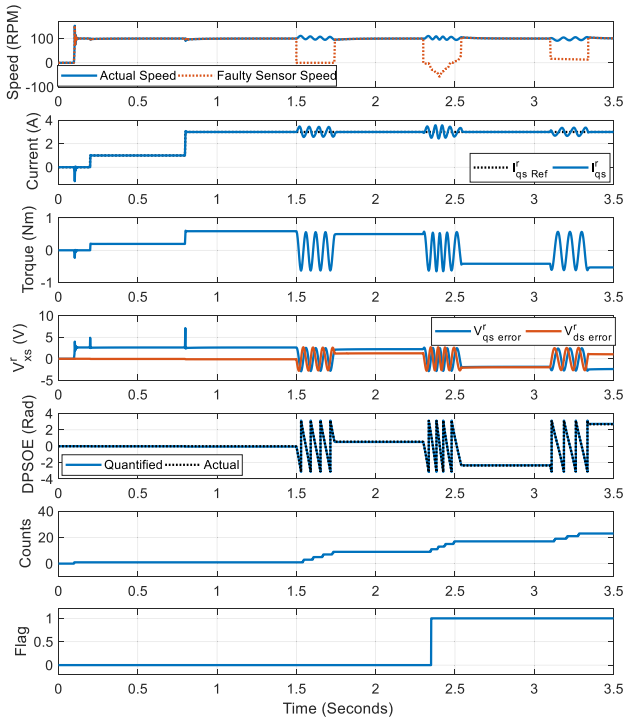

FIGURE 14. Simulation results of DPSOE detection at a constant speed of 100 RPM.

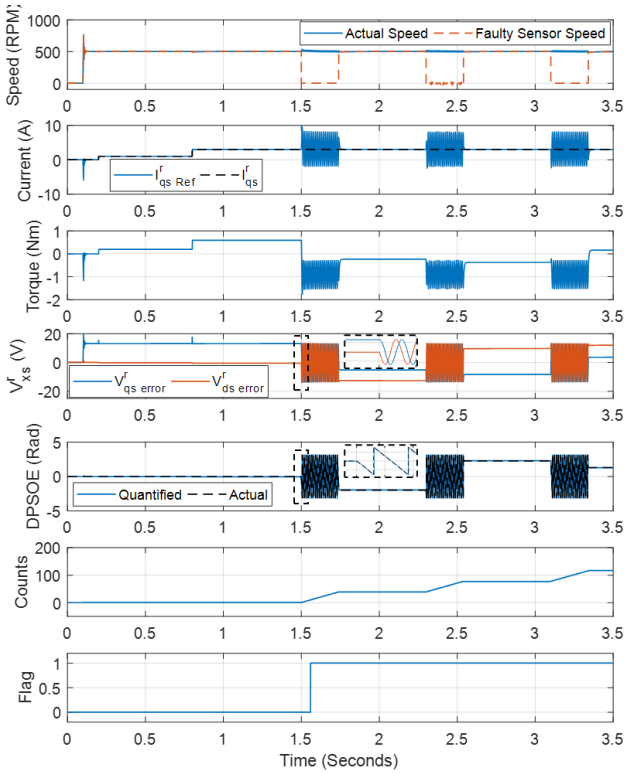

FIGURE 15. Simulation results of DPSOE detection at a constant speed of 500 RPM.

Figures 14 and 15 depict two simulation cases of DPSOE stick-slip and stuck fault scenarios and the detection of the fault using the proposed method. The fault- injected motor is operating as a torque regulate, while the dynamometer

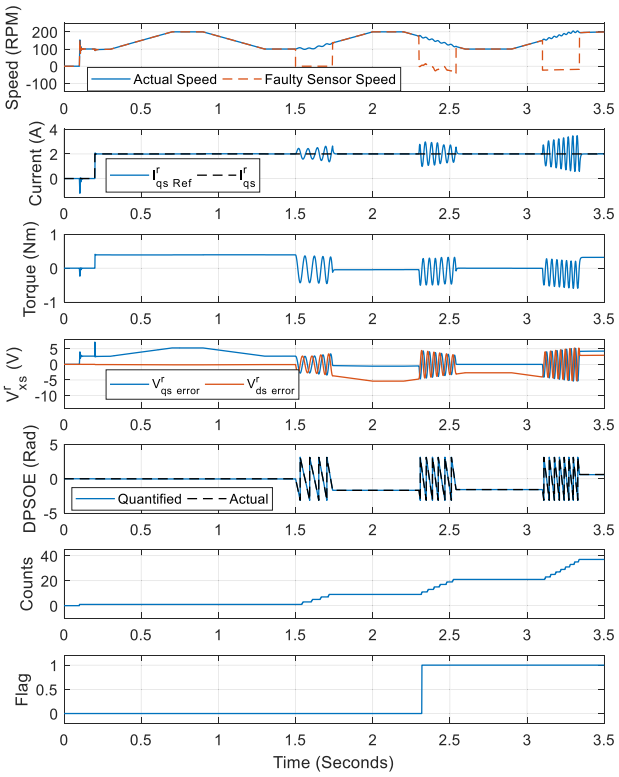

FIGURE 16. Simulation results of DPSOE detection under varying speed conditions (accelerations of 250rads^{-2}).

regulates the speed at 100RPM and 500RPM for the two sets of results, respectively. First subfigure of each figure shows the actual speed and the speed calculated based on the faulty position sensor. Second subfigure is showing the current reference and actual currents of the PMSM, followed by the motor torque output in subfigure 3. Subfigure 4 illustrates the rotor reference frame voltage error terms discussed in (20) and (21). The quantified and injected DPSOE are shown in the fifth subfigure. The DPSOE fault is introduced to the system at $t = 1.5$ *seconds*. The sixth and seventh subfigures show the counter value and the fault flag being set once the fault has persisted for a time period. These simulation results clearly illustrate how the proposed approach is capable of detecting a DPSOE condition when the system is operated at a constant speed. DPSOE detection under varying speed conditions is provided next.

Figures 16 and 17 illustrate simulation results on DPSOE detection in a torque regulated PMSM under varying speed conditions. Figure 16 corresponds with a low acceleration scenario whereas figure 17 is for a high acceleration scenario. Results shown in figure 16 and 17 subfigures depict the same signals as figures 14 and 15, with the exception of varying speed conditions while the current reference is being held constant at $I^r_{qs\_Ref} = 2A$ and $I^r_{ds\_Ref} = 0A$. DPSOE fault is introduced to the system at $t = 1.5$ *seconds*. Simulation results clearly demonstrate that the DPSOE can be detected using the proposed inverse tangent-based method under constant speed and varying speed conditions, with sufficient

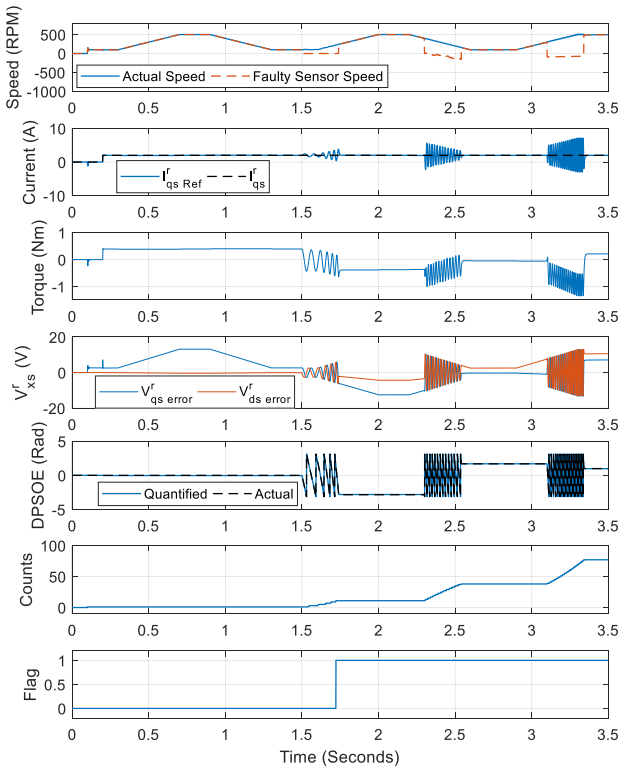

FIGURE 17. Simulation results of DPSOE detection under varying speed conditions (accelerations of 1000rads^{-2}).

TABLE 1. PMSM parameters.

Parameter	Value
Poles	10
Rated voltage	42V
Phase Resistance (r_s)	0.2239 Ω
Q-axis Inductance (L_q)	367.2 μH
Flux Linkage Constant (λ_m^{rr})	0.0122 V/(rads^{-1})

robustness preventing false positives during transient conditions at healthy states.

B. EXPERIMENTAL RESULTS ON DPSOE FAULT DIAGNOSIS

The following section presents experimental results on DPSOE detection. The experimental setup is shown in figure 4 along with PMSM parameters given in Table 1 below. The dual inverter drive board is controlled by the dSPACE DS1104 R&D system. A torque sensor placed between the two machines measures shaft torque. There are two optical encoders with one permanently mounted for true position and speed measurement while the other is used for DPSOE fault injection. Position and speed measurements from both sensors are observed simultaneously. The FOC PMSM operates with the healthy position signal during the healthy state and the system switches to the faulty position sensor when a DPSOE fault needs to be injected. The severity of the DPSOE (slowly varying vs rapidly varying nature) is adjusted by changing the setscrew mounting the faulty sensor to the coupling (figure 4).

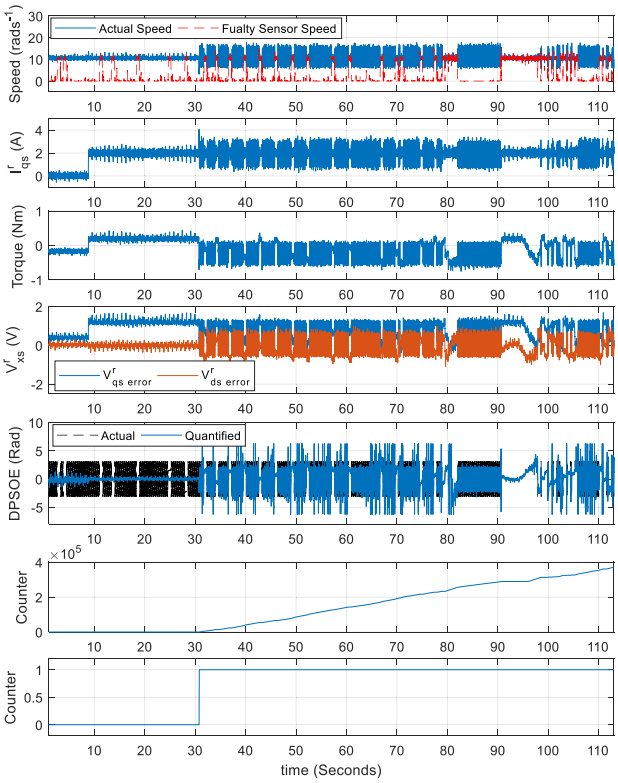

FIGURE 18. Experimental results of fast varying DPSOE detection at constant speed of 100RPM.

Figures 18 and 19 show DPSOE fault detection experimental results. In the experimental setup, the FOC controller is switched from the non-faulty (healthy) sensor to the faulty sensor signal as a means of fault injection. In figure 19, the switch from non-faulty to faulty sensor occurs slightly after $t = 30$ *seconds.* The first subfigure of each figure depicts the motor-dyno system speed based on the healthy and faulty sensors. In figure 18 the faulty sensor speed signal is seen dropping to zero intermittently due to complete detachment from the motor rotor and in figure 19, only slight variations of speed are seen due to small movements of the faulty sensor.

The second subfigure shows the regulation of the quadrature axis current under the fault condition. This clearly shows that an FOC system with feedback does *not fault out* or *stall* under a DPSOE, but rather continues to regulate currents in the erroneous reference frame resulting in unintended torque output from the machine. The actual torque output of the machine is shown in the third subfigure, where $I^r_{qs\_Ref} = 2A$ and $I^r_{ds\_Ref} = 0A$. Despite the constant current reference, torque can be seen fluctuating as the controller reference frame is constantly changing, resulting in rapid movement of the stator flux vector with respect to the rotor flux vector. Also, the reader should note the fluctuations seen in the measured currents in figures 18 and 19. These fluctuations in rotor reference frame current are caused by the closed-loop dynamics of the control system, adapting under continuously changing reference frame caused by DPSOE. The closed-loop current regulators are designed with a certain bandwidth in mind. However, step changes in the position sensor, cause

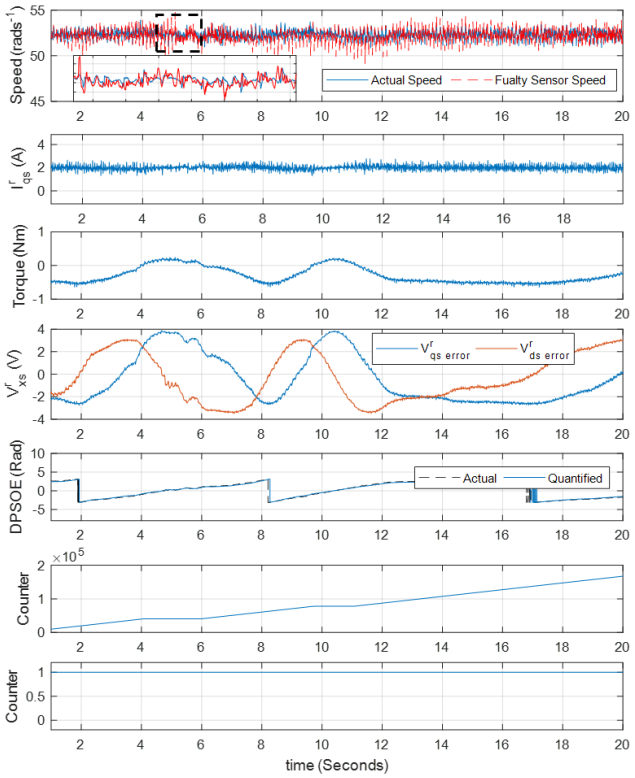

FIGURE 19. Experimental results of slow varying DPSOE detection at constant speed of 500RPM.

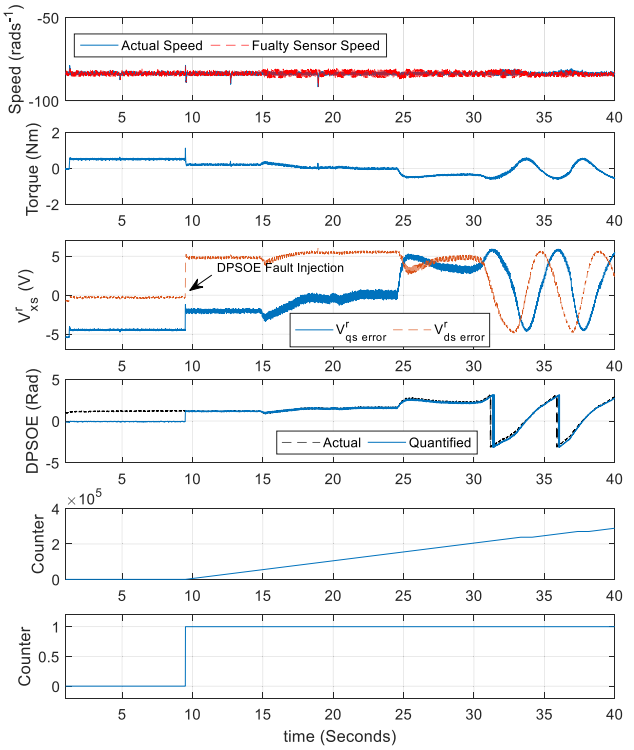

FIGURE 20. Experimental results of DPSOE detection at constant speed of 800RPM in counterclockwise motor rotation.

step changes in measured rotor reference frame currents, injecting high- frequency content into the closed loop system. As the current measurements change, the closed-loop system attempts to correct for the current. However, the P.I. regulators are unable to respond to the high-frequency content outside its designed bandwidth. Hence those high-frequency content reflects on the current measurement. This is evident when comparing the measured current signals in figures 18 and 19. In figure 19, the DPSOE is slowly varying allowing the current regulators to compensate. However, in figure 18, the rapidly changing DPSOE injects frequency content well beyond the current regulator bandwidth and hence the FOC system is unable to compensate.

Fourth subfigure illustrates quadrature and direct axis voltage errors utilized for DPSOE calculation followed by the quantified DPSOE in the fifth subfigure. The actual and the quantified DPSOE value tend to follow with reasonable accuracy and the accuracy can be seen improving at higher speeds as a result of higher induced EMF. The counter value used for DPSOE detection is shown in subfigure six and the fault flag status in subfigure seven. The fault flag can be seen rising (from zero to one) immediately after the DPSOE fault has been introduced to the system.

Additional experimental results are provided in figures 20 through 22. Figure 20 demonstrates DPSOE detection in the counterclockwise direction and at 800RPM motor speed. Figures 21 and 22 are for varying speed conditions with the current reference maintained constant. As mentioned earlier, the speed and position signals for healthy and faulty sensors are observed from the beginning and for fault injection, the position signal fed to the FOC system is changed from healthy to faulty. The fault injection point is indicated in each figure. The DPSOE quantification can be seen to follow the faulty offset error immediately triggering the fault flag, even under transient speed conditions. Both slow-varying and rapidly varying DPSOE cases are evaluated with sufficient accuracy. It is also noteworthy that the DPSOE algorithm does not indicate false positives under transient speeds when DPSOE is not present in the system, confirming the robustness of the proposed algorithm.

VI. ALTERNATE DPSOE DETECTION METHOD WITHOUT INVERSE TANGENT CALCULATION

Certain PMSM FOC drives are resource constrained especially in low-cost applications. An accurate inverse tangent calculation is either CPU resource heavy, storage heavy (for look-up table), or both. For example, on a Texas Instruments C2000 microprocessor, a single inverse tangent calculation takes approximately 90 floating point unit (FPU) cycles, whereas a multiplication of a floating-point number with a constant only consumes approximately 4 FPU cycles. Hence the authors propose the following method which does not require an inverse tangent calculation.

A Simulink implementation of the proposed DPSOE detection method is shown in figure 23. During a DPSOE fault, quadrature and direct axis voltages error in (20) and (21) oscillate from positive to negative. Therefore, comparing the

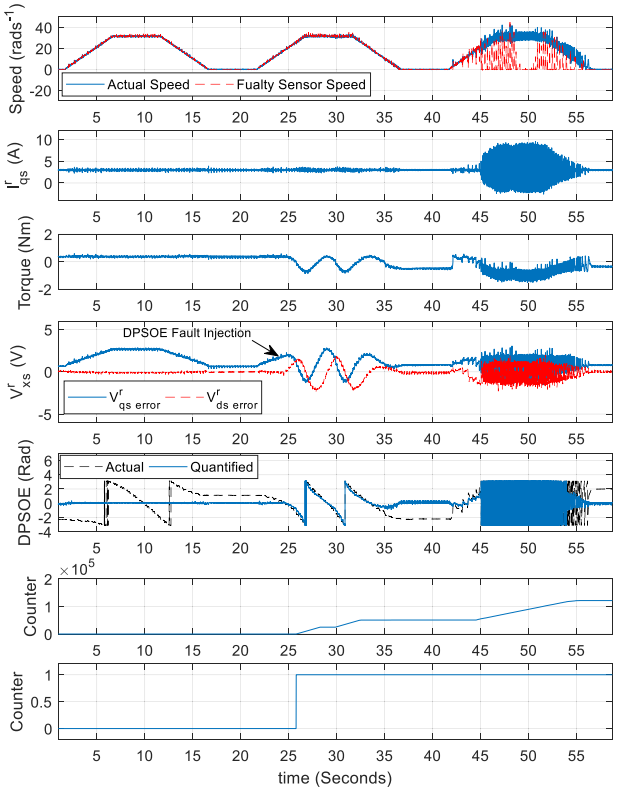

FIGURE 21. Experimental results of DPSOE detection under varying speed profile (Max Speed = 300RPM).

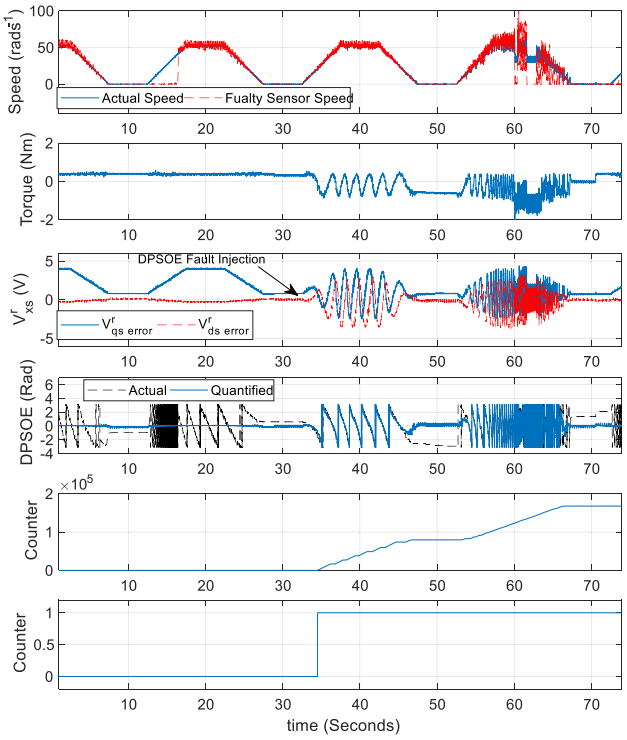

FIGURE 22. Experimental results of DPSOE detection under varying speed profile (Max Speed = 500RPM).

signal with respect to zero results in a binary signal for each axis. The binary signal is fed to a counter block that counts the total number of zero crossings for each of the signals

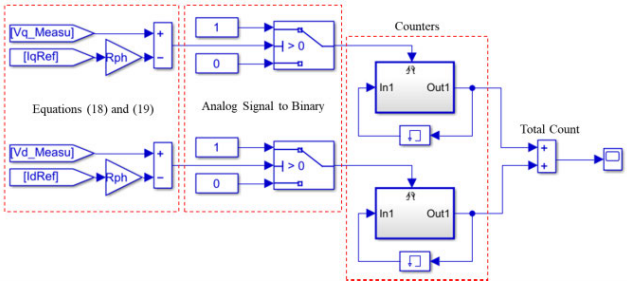

FIGURE 23. Block diagram of the DPSOE detection without inverse tangent calculation.

resulting in the total number of zero crossings. This serves as a method to detect DPSOE with little to no computational requirements. The total count value for detection mayvbe set to avoid false positives under transient conditions.

VII. CONCLUSION

Field-oriented controlled permanent magnet synchronous machines and drives are proliferating across many different energy conversion applications due to the numerous advantages of PMSMs. The use of sensed/sensored FOC is common in torque-controlled PMSM applications such as propulsion, traction, and steering applications due to high bandwidth requirements. However, a position sensor consists of mechanical interfaces that may incur faults due to vibration, shock, aging, or environmental conditions that occur in aforementioned applications introducing a dynamic position sensor offset error (DPSOE). This paper presents a comprehensive study of DPSOE, a modeling scheme to simulate various DPSOE conditions, and robust DPSOE detection methods. Two novel methods are presented with one with different levels of computational complexity. The proposed theoretical DPSOE detection scheme is supported by simulation and experimental results elaborating the practicality of the proposed approach. The fault model discussed is also a new contribution to the body of knowledge.

ACKNOWLEDGMENT

The authors would like to thank Ruth and Ted Braun Fellowship Program at Saginaw Valley State University for their continued support for research on electric machines, drives, and fault diagnosis of energy conversion systems. They also appreciate the support provided by Pat Graves, Melissa Woodward, Cara Shaw, Sandra Rasmussen, and Jaime Ayala of Saginaw Valley State University

REFERENCES

[1] J. Ebersberger, M. Hagedorn, M. Lorenz, and A. Mertens, "Potentials and comparison of inverter topologies for future all-electric aircraft propulsion," *IEEE J. Emerg. Sel. Topics Power Electron.*, vol. 10, no. 5, pp. 5264–5279, Oct. 2022, doi: 10.1109/JESTPE.2022.3164804.

[2] A. P. Thurlbeck and Y. Cao, "A mission profile-based reliability modeling framework for fault-tolerant electric propulsion," *IEEE Trans. Ind. Appl.*, vol. 58, no. 2, pp. 2312–2323, Mar. 2022, doi: 10.1109/TIA.2022.3144620.

[3] J. Harikumaran, G. Buticchi, G. Migliazza, V. Madonna, P. Giangrande, A. Costabeber, P. Wheeler, and M. Galea, "Failure modes and reliability oriented system design for aerospace power electronic converters," *IEEE Open J. Ind. Electron. Soc.*, vol. 2, pp. 53–64, 2021, doi: 10.1109/OJIES.2020.3047201.

[4] J. L. F. Daya, P. Sanjeevikumar, F. Blaabjerg, P. W. Wheeler, and J. O. Ojo, "Implementation of wavelet-based robust differential control for electric vehicle application," *IEEE Trans. Power Electron.*, vol. 30, no. 12, pp. 6510–6513, Dec. 2015, doi: 10.1109/TPEL.2015.2440297.
[5] S. Haggag, D. Alstrom, S. Cetinkunt, and A. Egelja, "Modeling, control, and validation of an electro-hydraulic steer-by-wire system for articulated vehicle applications," *IEEE/ASME Trans. Mechatronics*, vol. 10, no. 6, pp. 688–692, Dec. 2005, doi: 10.1109/TMECH.2005.859838.
[6] A. Benevieri, M. Marchesoni, M. Passalacqua, and L. Vaccaro, "Experimental low-speed performance evaluation and comparison of sensorless passive algorithms for SPMSM," *IEEE Trans. Energy Convers.*, vol. 37, no. 1, pp. 654–664, Mar. 2022, doi: 10.1109/TEC.2021.3101583.
[7] C. Wu, Z. Chen, and Q. Chen, "An optimized asymmetric pulsewidth modulation for sensorless control of permanent magnet synchronous machines," *IEEE Trans. Ind. Electron.*, vol. 69, no. 2, pp. 1389–1399, Feb. 2022, doi: 10.1109/TIE.2021.3060676.
[8] M. A. G. Moghadam and F. Tahami, "Sensorless control of PMSMs with tolerance for delays and stator resistance uncertainties," *IEEE Trans. Power Electron.*, vol. 28, no. 3, pp. 1391–1399, Mar. 2013, doi: 10.1109/TPEL.2012.2207405.
[9] J. Fang, X. Zhou, and G. Liu, "Instantaneous torque control of small inductance brushless DC motor," *IEEE Trans. Power Electron.*, vol. 27, no. 12, pp. 4952–4964, Dec. 2012, doi: 10.1109/TPEL.2012.2193420.
[10] S. S. Kuruppu, "Open-loop self-calibration of position sensor offset in SM-PMSM drive systems," *IEEE Trans. Instrum. Meas.*, vol. 70, pp. 1–7, 2021, doi: 10.1109/TIM.2021.3065749.
[11] R. Ramakrishnan, A. Gebregergis, M. Islam, and T. Sebastian, "Effect of position sensor error on the performance of PMSM drives for low torque ripple applications," in *Proc. Int. Electr. Mach. Drives Conf.*, May 2013, pp. 1166–1173, doi: 10.1109/IEMDC.2013.6556307.
[12] S. S. Kuruppu, "Position sensor harmonics influence on highly integrated field oriented controlled PMSM drive torque output," in *Proc. IEEE Transp. Electrific. Conf. Expo (ITEC)*, Jun. 2021, pp. 427–433, doi: 10.1109/ITEC51675.2021.9490171.
[13] S. S. Kuruppu and Y. Zou, "Static position sensor bias fault diagnosis in permanent magnet synchronous machines via current estimation," *IEEE/ASME Trans. Mechatronics*, vol. 26, no. 2, pp. 888–896, Apr. 2021, doi: 10.1109/TMECH.2020.3010898.
[14] R. Ghimire, C. Zhang, and K. R. Pattipati, "A rough set-theory-based fault-diagnosis method for an electric power-steering system," *IEEE/ASME Trans. Mechatronics*, vol. 23, no. 5, pp. 2042–2053, Oct. 2018, doi: 10.1109/TMECH.2018.2863119.
[15] M. Bahari and F. Tootoonchian, "Proposal of a fault-tolerance technique for 1-ph open circuit fault in resolvers," *IEEE Sensors J.*, vol. 21, no. 14, pp. 15987–15992, Jul. 2021, doi: 10.1109/JSEN.2021.3076173.
[16] G. De Donato, G. Scelba, M. Pulvirenti, G. Scarcella, and F. G. Capponi, "Low-cost, high-resolution, fault-robust position and speed estimation for PMSM drives operating in safety-critical systems," *IEEE Trans. Power Electron.*, vol. 34, no. 1, pp. 550–564, Jan. 2019, doi: 10.1109/TPEL.2018.2820042.
[17] J. Lu, Y. Hu, J. Liu, X. Zhang, H. Wen, and Z. Wang, "Position sensor fault detection of IPMSM using single DC-bus current sensor with accuracy uncertainty," *IEEE/ASME Trans. Mechatronics*, vol. 24, no. 2, pp. 753–762, Apr. 2019, doi: 10.1109/TMECH.2019.2892954.
[18] I. Jlassi and A. J. M. Cardoso, "A single method for multiple IGBT, current, and speed sensor faults diagnosis in regenerative PMSM drives," *IEEE J. Emerg. Sel. Topics Power Electron.*, vol. 8, no. 3, pp. 2583–2599, Sep. 2020, doi: 10.1109/JESTPE.2019.2918062.
[19] G. Scelba, G. De Donato, M. Pulvirenti, F. Giulii Capponi, and G. Scarcella, "Hall-effect sensor fault detection, identification, and compensation in brushless DC drives," *IEEE Trans. Ind. Appl.*, vol. 52, no. 2, pp. 1542–1554, Mar. 2016, doi: 10.1109/TIA.2015.2506139.

SANDUN S. KURUPPU (Senior Member, IEEE) received the B.S. degree in electrical and electronics engineering from the University of Peradeniya, Sri Lanka, in 2007, and the M.S. and Ph.D. degrees from Purdue University, West Lafayette, IN, USA, in 2010 and 2013, respectively.

He is currently an Associate Professor of electrical and computer engineering and the Director of the Transportation Electrification and Applied Mechatronics Laboratory, Western Michigan University (WMU), Kalamazoo, MI, USA. Prior to his current position, he was with Saginaw Valley State University, Nexteer Automotive, Texas Instruments Kilby Labs, and Delphi Electronics and Safety. His current research interests include fault prognostics, diagnostics, localization, mitigation in mechatronic systems, power electronics, vehicle stability control, and extremum seeking controls for traction applications.

Dr. Kuruppu was a recipient of the Ruth and Ted Braun Fellowship and the Award for Excellence for Online Teaching from Saginaw Valley State University, in 2021. He was the Student Activities Chair of the IEEE ECCE, in 2022. He is an Associate Editor of IEEE Power Electronics Society, Educational Videos on Power Electronics.

SUNIL G. ABEYRATNE (Senior Member, IEEE) was born in Kandy, Sri Lanka. He received the B.Sc.Eng. degree in electrical and electronics engineering from the University of Peradeniya, Peradeniya, Sri Lanka, in 1987, and the M.Eng. and Ph.D. degrees from Gifu University, Gifu, Japan, in 1992 and 1997, respectively.

From 1987 to 1988, he was an Instructor with the Department of Electrical and Electronic Engineering, University of Peradeniya. In 1998, he joined Colombo Dockyard Ltd., as an Electrical and Electronic Engineer, where he was until January 2000. He was a Researcher with the Wisconsin Power Electronics Research Center, University of Wisconsin–Madison, Madison, WI, USA, from 1992 to 1994. From 1997 to 1998, he was a Software Engineer with Total Office Operations, Japan. He joined the University of Peradeniya as a Senior Lecturer, in 1999. He has been with Toshiba Schneider Inverter Corporation, Design and Development Group, Mie, Japan, as a Researcher/Trainee, in 2001. Since 2017, he has been a Professor with the Faculty of Engineering, University of Peradeniya.

SANDUN HETTIARACHCHI received the B.Sc. degree in electrical and electronic engineering from the University of Peradeniya, Sri Lanka, in 2016. He is currently pursuing the master's degree in automation and control with the Technical University of Kaiserslautern, Germany. He has held a temporary instructor position with the Department of Electrical and Electronic Engineering, Faculty of Engineering, University of Peradeniya, for several years. His research interests include electrical machines, power electronics, and their control systems.